I&EC research
Industrial & Engineering Chemistry Research

Article

pubs.acs.org/IECR

Photo-Fenton Degradation of the Herbicide 2,4-Dichlorophenoxyacetic Acid in Laboratory and Solar Pilot-Plant Reactors

Leandro O. Conte,[†] Jorgelina Farias,[†] Enrique D. Albizzati,[‡] and Orlando M. Alfano*[,†]

[†]Instituto de Desarrollo Tecnológico para la Industria Química (INTEC), Consejo Nacional de Investigaciones Científicas y Técnicas (CONICET) and Universidad Nacional del Litoral (UNL), Güemes 3450, 3000 Santa Fe, Argentina.

[‡]Facultad de Ingeniería Química, Universidad Nacional del Litoral (UNL), Santiago del Estero 2654, 3000 Santa Fe, Argentina.

ABSTRACT: A theoretical and experimental study of a pilot-plant solar reactor for the photo-Fenton degradation of the herbicide 2,4-dichlorophenoxyacetic acid (2,4-D) in aqueous solution is presented. Initially, a kinetic model is proposed to obtain the reaction rates of 2,4-D, the main intermediate (2,4-dichlorophenol), and the hydrogen peroxide. The kinetic study was performed in a well-stirred tank laboratory reactor. The effects of ferric salt initial concentrations, hydrogen peroxide to 2,4-D initial concentration ratios, reaction temperatures, and radiation levels are studied. The proposed kinetic model and the experimental data are used to estimate the kinetic parameters, applying a nonlinear regression procedure. Afterward, the kinetic model is used to predict the reactant concentrations during the photo-Fenton degradation in a pilot-plant solar reactor designed to capture the UV/visible/IR solar radiation. The solar reactor was able to reach a complete degradation of the 2,4-D and 2,4-dichlorophenol after 60 min, and a total organic carbon conversion of 98.9% after 210 min.

1. INTRODUCTION

Advanced oxidation processes (AOPs) are based on the generation of reactive species such as hydroxyl radicals, which are able to oxidize and mineralize a great variety of toxic and nonbiodegradable compounds as a result of their high reactivity and low selectivity. Particularly, the photo-Fenton process is useful to destroy several pollutants such as biologically nondegradable compounds that cannot be eliminated by means of well-known wastewater treatments.[1] This reaction produces highly oxidant species from the combination of iron salts with hydrogen peroxide under artificial or sunlight UV−visible radiation.[2] It is known that high temperatures can increase the dark or Fenton reaction rate.[3−5] It has been also reported that the degradation intermediates of aromatic compounds, such as quinone and hydroquinone intermediates, can enhance the production of ferrous species through dark reactions.[6−9]

Several attempts have been made employing sunlight as a source of energy to investigate the photo-Fenton remediation of wastewater containing a variety of toxic compounds.[10−12] Using this process, the degradation of several aqueous organic compounds has been recently investigated: persistent pharmaceuticals,[13,14] commercial pesticides,[15−17] nonbiodegradable azo dyes,[18] and emerging contaminants at low concentrations,[19] among others.

As a result of agriculture activities, large volumes of water containing high quantities of pesticides are generated by the cleaning processes of irrigation equipments and empty containers, producing a negative environmental impact. One of the pesticides frequently employed in the control of broadleaf weeds is 2,4-dichlorophenoxyacetic acid (2,4-D); it is one of the most widely used herbicides that is known to be have a high level of toxicity. Its relatively high solubility in water facilitates its migration to natural courses, where it may last for several weeks due to its long mean lifetime.

The photo-Fenton solar process was successfully applied to treat water containing a variety of agrochemicals coming from these agriculture activities.[10] Very recently, a new pilot-plant solar reactor for the photo-Fenton treatment of a model pollutant (formic acid) in aqueous solution was presented.[20] This hybrid unit was designed and built to capture the UV/visible and near-infrared solar radiation, yielding higher degradation rates of the model compound. An experimental temperature increase up to 25 °C was obtained with this solar reactor at the end of the irradiated runs (480 min). Also, for a reaction time of 180 min and a low iron concentration of 3.4 ppm, the authors found that the combined effect of the photochemical and thermal solar radiation was able to degrade 98.2% of the initial pollutant concentration.

The aim of this work is to study the photo-Fenton degradation of the herbicide 2,4-D in aqueous solution, using the new pilot-plant solar reactor. First, a kinetic model derived from a reaction sequence is proposed; this model was employed to predict the concentrations of the 2,4-D, the main intermediate 2,4-dichlorophenol (DCP), and the hydrogen peroxide in an isothermal, well-stirred tank laboratory reactor irradiated from the bottom. Using the kinetic model results and the experimental data, the corresponding kinetic parameters were estimated between 20 and 50 °C, for low ferric iron concentrations and different hydrogen peroxide to 2,4-D initial molar ratios. Afterward, the kinetic model was employed to predict the reacting

Received: October 10, 2011
Revised: February 11, 2012
Accepted: February 14, 2012
Published: February 14, 2012

dx.doi.org/10.1021/ie2023228 | *Ind. Eng. Chem. Res.* 2012, 51, 4181−4191

species concentrations during the photo-Fenton degradation in the pilot-plant solar reactor, under different experimental conditions. Finally, predicted and experimental species concentrations, reaction temperatures, and UV and total broadband solar radiation fluxes as a function of time, were compared.

2. KINETIC MODEL

The proposed kinetic model for the Fenton and photo-Fenton degradation of 2,4-D is based on the reaction sequence reported by Sun and Pignatello,[21,22] Brillas et al.,[23] and Pignatello et al.[2] The reaction scheme is illustrated in Table 1.

Table 1. Reaction Scheme for 2,4-D Degradation

number	reaction step	constant
0	$Fe(III) + H_2O \rightarrow Fe(II) + OH^\bullet + H^+$	$\Phi_{Fe(II),\lambda}$
1	$Fe(III) + H_2O_2 \rightarrow Fe(II) + H^+ + HO_2^\bullet$	k_1
2	$Fe(II) + H_2O_2 \rightarrow Fe(III) + OH^- + HO^\bullet$	k_2
3	$H_2O_2 + HO^\bullet \rightarrow HO_2^\bullet + H_2O$	k_3
4	$Fe(II) + HO^\bullet \rightarrow Fe(III) + OH^-$	k_4
5	$H_2O_2 + HO_2^\bullet \rightarrow HO^\bullet + H_2O + O_2$	k_5
6	$2HO^\bullet \rightarrow H_2O_2$	k_6
7	$2HO_2^\bullet \rightarrow H_2O_2 + O_2$	k_7
8	$HO_2^\bullet + HO^\bullet \rightarrow H_2O + O_2$	k_8
9	$Fe(III) + HO_2^\bullet \rightarrow Fe(II) + H^+ + O_2$	k_9
10	$Fe(II) + HO_2^\bullet + H^+ \rightarrow Fe(III) + H_2O_2$	k_{10}
11	$2,4\text{-D} + HO^\bullet \rightarrow DCP$	k_{11}
12	$DCP + OH^\bullet \rightarrow QH_2$	k_{12}
13	$QH_2 + HO^\bullet \rightarrow$ products	k_{13}
14	$QH_2 + Fe(III) \rightarrow Fe(II) + QH^\bullet + H^+$	k_{14}
15	$QH^\bullet + Fe(III) \rightarrow Q + Fe(II) + H^+$	k_{15}

The degradation rate expressions of 2,4-D, its main intermediate DCP, and hydrogen peroxide (P) are derived from the following assumptions: (i) radical−radical termination reactions are neglected as compared with the propagation reactions; (ii) reaction of hydroxyl radical with Fe(II) is neglected due to the low ferric ion concentrations;[2] (iii) reaction step 5 is slow compared to others of $HO_2^\bullet$ and can be neglected;[2] (iv) reaction of hydroxyl radical with quinone intermediates (QH_2) is neglected as compared with Fe(III) reactions;[9] (v) steady-state approximation (SSA) may be applied for highly reactive radicals, such as $OH^\bullet$ and $QH^\bullet$; (vi) the ferrous ion and quinone intermediate concentrations are very low; and (vii) the oxygen concentration is always in excess. With these assumptions, the following reaction rate expressions can be derived (Appendix A):

$$\begin{bmatrix} R_{2,4\text{-D}}(x,t) \\ R_{DCP}(x,t) \\ R_P(x,t) \end{bmatrix} = \begin{bmatrix} R^T_{2,4\text{-D}}(t) \\ R^T_{DCP}(t) \\ R^T_P(t) \end{bmatrix} + \bar{\Phi}_{Fe(II)} \sum_\lambda e^a_\lambda(x) \begin{bmatrix} \frac{-2}{\delta} \\ \frac{2}{\delta}\left(1 - K_{DCP}\frac{C_{DCP}}{C_{2,4\text{-D}}}\right) \\ -\frac{1}{\delta}\left(1 + 3K_{DCP}\frac{C_{DCP}}{C_{2,4\text{-D}}} + 3K_{III}\frac{C_P}{C_{2,4\text{-D}}}\right) \end{bmatrix} \quad (1)$$

In eq 1, the following kinetic parameters have been defined:

$$\delta = 1 + K_{III}\frac{C_P}{C_{2,4\text{-D}}} - K_{DCP}\frac{C_{DCP}}{C_{2,4\text{-D}}} \quad (2)$$

$$K_{III} = \frac{k_3}{k_{11}}, \qquad K_{DCP} = \frac{k_{12}}{k_{11}} \quad (3)$$

Note that eq 1 for the three reacting species can be written by using the following matrix representation:

$$\mathbf{R}(x,t) = \mathbf{R}^T(t) + \bar{\Phi}_{Fe(II)} \sum_\lambda e^a_\lambda(x)\, \mathbf{\Gamma}(t) \quad (4)$$

The first term on the right-hand side of eq 1 or 4, which corresponds to the thermal reaction rate, may be represented by the matrix expression

$$\begin{bmatrix} R^T_{2,4\text{-D}}(t) \\ R^T_{DCP}(t) \\ R^T_P(t) \end{bmatrix} = K_1 C_{Fe^{3+}} C_P \begin{bmatrix} -\frac{1}{\delta} \\ \frac{1}{\delta}\left(1 - K_{DCP}\frac{C_{DCP}}{C_{2,4\text{-D}}}\right) \\ -\left(\frac{2 + 3K_{III}C_P/C_{2,4\text{-D}}}{\delta}\right) \end{bmatrix} \quad (5)$$

In eq 5, the following kinetic parameter has been defined: $K_1 = k_1$.

3. LABORATORY PHOTOREACTOR

3.1. Reactor Model. Kinetic studies were performed in an isothermal, well-stirred tank reactor irradiated from the bottom. The mass balance is given by the following set of first-order, ordinary differential equations

$$\frac{d}{dt}\mathbf{C}(t) = \mathbf{R}^T(t) + \bar{\Phi}_{Fe(II)}\langle e^a(x)\rangle_{V_R}\mathbf{\Gamma}(t) \quad (6)$$

with the initial conditions

$$\mathbf{C} = \mathbf{C}^0 \qquad t = 0 \quad (7)$$

Note that the required reaction rate expressions to replace in eq 6 are given by eqs 1−3 and 5.

For the numerical evaluation of the second term on the right-hand side of eq 6, it is necessary to know the value of the local volumetric rate of photon absorption (LVRPA) at every point inside the reactor and then to compute the LVRPA averaged over the reactor volume. Following the assumptions proposed by Alfano et al.[24] for a similar laboratory photoreactor, a one-dimensional radiation field model has been used in this work to calculate the monochromatic LVRPA as a function of the spatial coordinate x. Thus,

$$e^a_\lambda(x) = \kappa_\lambda q_w f_\lambda \exp(-\kappa_{T,\lambda} x) \quad (8)$$

Here q_w is the spectral net radiation flux at the reactor wall, f_λ is the normalized spectral distribution of the lamp output power, κ_λ is the volumetric absorption coefficient of the reacting species, and $\kappa_{T,\lambda}$ is the volumetric absorption coefficient of the medium.

To solve eq 8, it is considered that $Fe(OH)^{2+}$ is the ferric species dominant at pH 3[25] and that the radiation absorption of

dx.doi.org/10.1021/ie2023228 | Ind. Eng. Chem. Res. 2012, 51, 4181−4191

Table 2. Coded variables, operating conditions and percent conversions of 2,4-D (t = 30 min) and TOC (t = 120 min)

	coded variables									
N	X_1	X_2	X_3	X_4	T (°C)	$C^0_{Fe(III)}$(ppm)	R	Rad	$X^{30}_{2,4\text{-D}}$ (%)	X^{120}_{TOC} (%)
1	−1	1	0	−1	20	5	28.5	0	42.3	20.0
2	−1	0	−1	−1	20	3	7	0	22.1	12.0
3	−1	−1	−1	−1	20	1	7	0	3.5	12.8
4	−1	−1	1	−1	20	1	50	0	5.5	5.8
5	−1	−1	0	1	20	1	28.5	1	81.4	88.0
6	−1	1	1	1	20	5	50	1	100	83.7
7	−1	1	−1	1	20	5	7	1	97.5	73.7
8	1	−1	0	−1	50	1	28.5	0	96.7	36.6
9	1	1	−1	−1	50	5	7	0	100	46.2
10	1	1	1	−1	50	5	50	0	100	34.6
11	0	−1	−1	1	35	1	7	1	100	50.5
12	1	1	0	1	50	5	28.5	1	99.2	85.6
13	1	−1	1	1	50	1	50	1	99.6	86.9
14	0	−1	1	0	35	1	50	0.5	79.8	78.2
15	1	−1	−1	0	50	1	7	0.5	100	47.4

hydrogen peroxide and ferrous ion is negligible for wavelengths greater than 300 nm. Consequently,

$$\kappa_{T,\lambda} = \sum_i \alpha_{i,\lambda} C_i \cong \alpha_{Fe(OH)^{2+},\lambda} C_{Fe(OH)^{2+}} \tag{9}$$

Here, the molar absorptivity of the absorbing species $[\alpha_{Fe(OH)^{2+}}]$ is a function of the wavelength λ.

Since the lamp output power and the optical properties of the reactants are functions of wavelength, an integration over all the useful wavelengths must be performed to compute $e^a(x)$:

$$e^a(x) = \int_{\lambda_{min}}^{\lambda_{max}} e^a_\lambda(x)\, d\lambda \cong \sum_\lambda e^a_\lambda(x) \tag{10}$$

3.2. Experiments. The employed apparatus was an isothermal, well-stirred tank photoreactor, irradiated from the bottom with a low-pressure mercury-vapor fluorescent lamp (Philips TL 40W/09 N) placed at the focal axis of a parabolic reflector. More details on this laboratory photoreactor can be found elsewhere.[26]

For the experimental design, a D-optimal design method was adopted, and the following operating variables were considered: (i) reaction temperatures, T (°C) = [20, 50]; (ii) iron salt concentrations, $C^0_{Fe^{3+}}$ (ppm) = [1, 5]; (iii) hydrogen peroxide to 2,4-D initial concentration ratios, R = [7, 50]; and (iv) three irradiation levels, Rad = [0, 0.5, 1]. To avoid the precipitation of iron compounds during the experimental runs, low iron concentrations (≤5 ppm) and reaction temperatures (≤50 °C) were employed in the present work.[27,5] These working variables are coded as X_1, X_2, X_3, and X_4, respectively. A quadratic model with interactions and a minimum number of experimental runs was adopted. The following grid and restrictions were selected

$$X_i = \left[-1{:}\ \frac{1}{16}{:}\ 1\right] \quad (i = 1,\ 2,\ 3,\ \text{and}\ 4) \tag{11}$$

where

$$X_4 = [-1 \quad 0 \quad 1] \tag{12}$$

Table 2 shows the coded variables and operating conditions for the experimental runs, for a 2,4-D initial concentration of 0.13 mM and pH 3. The percent conversion of 2,4-D after a reaction time t = 30 min and of the total organic carbon (TOC) at t = 120 min are also presented. For experiments at intermediate irradiation level, a specially constructed neutral density filter made of UVA transparent thin films was placed between the emitting system and the bottom of the reactor.[28]

The experimental procedure began when ferric sulfate (Carlo Erba, RPE) and 2,4-D (Merck, 99%) solutions were added to the reactor with distilled water, and concentrated sulfuric acid was used to adjust pH to 3. A shutter located between the illuminating system and the reactor bottom helped to obtain the specified working conditions of temperature and lamp operation. Then, hydrogen peroxide (Carlo Erba, ACS, 30%P) solution was added to the reactor and the first sample was withdrawn (reaction time equal to zero). Finally, the shutter was removed to start the irradiated experiments.

As soon as the sample was withdrawn, the Fenton reaction was stopped instantaneously by adding methanol. Then, 2,4-D and its reaction intermediates were analyzed by HPLC using a Waters chromatograph equipped with a LC-18 Supelcosil reversed phase column (Supelco). The eluent was a binary mixture of distilled water (containing 1% v/v acetic acid) and acetonitrile in proportion 50:50.[29] The eluent flow rate was 1 $cm^3\ min^{-1}$. Detection was done at 236 and 280 nm. Hydrogen peroxide was analyzed with a modified iodimetric technique and ferrous ions with absorbance measurements of the Fe(II)−phenantroline complex. In addition, total carbon measurements were performed by employing a Shimadzu TOC-5000A analyzer.

3.3. Evaluation of the Kinetic Parameters. An optimization procedure was employed to provide the values of parameters that minimize the differences between model predictions and experimental data of 2,4-D, DCP, and hydrogen peroxide concentrations. The theoretical values were obtained solving the system of ordinary differential equations presented in section 3.1.

To compute the radiation field inside the photoreactor, the net radiative flux at the reactor bottom was evaluated by ferrioxalate actinometry.[30] From these experiments, the following values were determined: q_w = 15.9 neinstein $cm^{-2}\ s^{-1}$ (high irradiation level) and q_w = 5.41 neinstein $cm^{-2}\ s^{-1}$ (intermediate irradiation level). The spectral data for the molar absorptivity of the absorbing species ($\alpha_{Fe(OH)^{2+}}$) were obtained from Faust and Hoigné,[25] and the normalized spectral

dx.doi.org/10.1021/ie2023228 | Ind. Eng. Chem. Res. 2012, 51, 4181−4191

distribution of the lamp output power (f_λ) was provided by the lamp manufacturer.

According to Schwaab and Pinto,[31] to preserve a statistic meaning of the correlation, a linear regression should not be applied. Consequently, in this paper the Arrhenius equation was introduced in the reaction rate expressions, and all the kinetic parameters were estimated simultaneously by using the whole set of experimental data. Specifically, a nonlinear, Newton Gauss−Marquardt optimization algorithm was applied to estimate the Arrhenius parameters: the frequency (or pre-exponential) factor and the activation energy.[5] On the other hand, to avoid the high parameter correlation between the pre-exponential factors and the activation energies, and the computational effort required to minimize the objective function, a reparameterization of the Arrhenius equation and definition of a reference temperature (T_{ref} = 308 K) was employed.[31,5] Thus, K_1 was defined as

$$K_1 = \exp\left[A_1 + B_1\left(\frac{T - T_{ref}}{T}\right)\right] \quad (13)$$

The parameters of the reparameterized equation can be related to the parameters of the conventional Arrhenius equation by

$$A_1 = \ln(K_{ref}) = \ln(K_{\infty,1}) - \frac{E_1}{R'T_{ref}} \quad (14)$$

$$B_1 = \frac{E_1}{R'T_{ref}} \quad (15)$$

where K_{ref} is the kinetic constant at the reference temperature.

Estimated values of the kinetic parameters are shown in Table 3. The differences between computed results and experimental data were calculated by means of the root-mean-square error (RMSE); for 2,4-D, DCP and hydrogen peroxide concentrations they were 1.16×10^{-2} , 0.78×10^{-2}, and 0.38 mM, respectively.

Table 3. Estimated Values of Kinetic Parameters

reparameterized parameters			parameters		
A_1	−0.355	±0.014	$K_{\infty,1}$	0.707	$M^{-1}\ s^{-1}$
B_1	32.67	±1.000	E_1	83.66	kJ mol^{-1}
$\ln(K_{III})$	−3.324	±0.046	K_{III}	0.036	
$\ln(K_{DCP})$	2.073	±0.461	K_{DCP}	7.951	
$\ln(\bar{\Phi}_{Fe(II)})$	−1.439	±0.058	$\bar{\Phi}_{Fe(II)}$	0.237	mol $einstein^{-1}$

Figure 1 presents model predictions and experimental data of the time evolution of 2,4-D, DCP, and hydrogen peroxide relative concentrations for experiments at 20 °C and for $C^0_{2,4\text{-}D}$= 0.13 mM. When Figure 1a for $C_{Fe(III)}$ = 5 ppm and R = 28.5 is compared with Figure 1b for $C_{Fe(III)}$ = 1 ppm and R = 50, an important 2,4-D conversion decrease is observed for the Fenton reaction; for example, $X_{2,4\text{-}D}$ at t = 30 min was 42.3% and 5.5%, respectively (see Table 2, runs 1 and 4). Here it should be stressed the important effect of the ferric ion initial concentration on the Fenton reaction at low temperatures (20 °C); also note that the positive effect produced by a higher ferric ion concentration could not be counterbalanced by the corresponding increase of the molar ratio R from 28.5 to 50.

On the other side, a significant 2,4-D conversion enhancement is obtained in Figure 1c for the photo-Fenton system (run 5). A pollutant conversion of 81.4% after 30 min is observed for the lowest ferric salt concentration ($C_{Fe(III)}$ = 1 ppm), an intermediate hydrogen peroxide to pollutant concentration ratio (R = 28.5), and the lowest temperature (20 °C). In addition, Figure 1c shows an almost complete degradation of 2,4-D after 60 min.

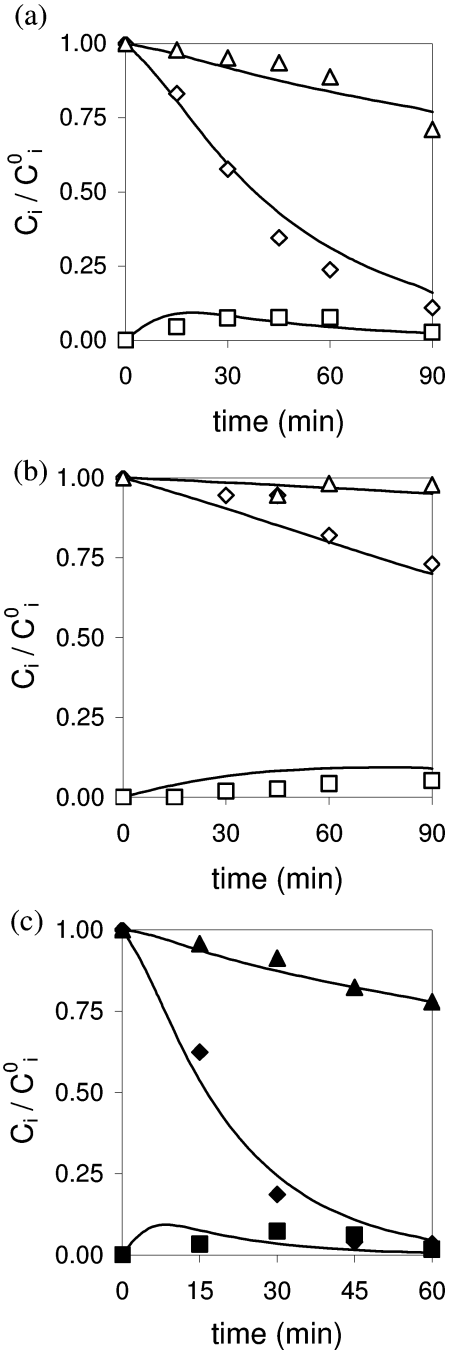

Figure 1. Predicted (lines) and experimental (symbols) relative concentrations vs time, for $C^0_{2,4\text{-}D}$ = 0.13 mM and 20 °C: (a) Fenton reaction, R = 28.5 and $C_{Fe(III)}$ = 5 ppm; (b) Fenton reaction, R = 50 and $C_{Fe(III)}$ = 1 ppm; and (c) photo-Fenton reaction, R = 28.5 and $C_{Fe(III)}$ = 1 ppm. Keys for experimental concentrations: 2,4-D (◇), DCP (□) and hydrogen peroxide (Δ); Fenton (◇, □, Δ), photo-Fenton (◆, ■, ▲).

Predicted and experimental results for Fenton and photo-Fenton reactions are also represented in Figure 2. It shows a 3-D plot of 2,4-D conversion at t = 30 min as a function of the reaction temperature and ferric ion concentration, for the

dx.doi.org/10.1021/ie2023228 | Ind. Eng. Chem. Res. 2012, 51, 4181−4191

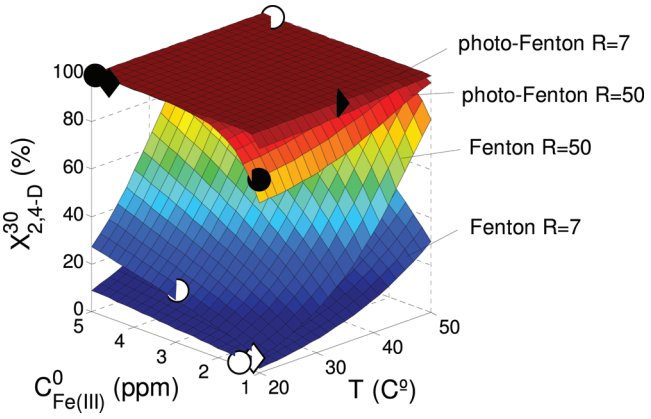

Figure 2. Predicted (surfaces) and experimental (symbols) 2,4-D conversions after 30 min vs reaction temperatures and ferric iron concentrations, for R = 7 and 50. Keys: Fenton (open symbols), photo-Fenton (filled symbols), R = 50 (circles), R = 7 (diamonds).

lowest (7) and highest (50) values of R. Notice that, for low and intermediate reaction temperatures, the photo-Fenton reaction always produces a 2,4-D conversion higher than that achieved for the Fenton (or dark) reaction. However, as temperature is increased, the differences between Fenton and photo-Fenton conversions of 2,4-D are noticeably reduced; for instance, at T = 50 °C, R = 50, and $C_{Fe(III)}$ = 5 ppm, these 2,4-D conversion differences are insignificant.

For the photo-Fenton reaction, it is noted that for the highest hydrogen peroxide to pollutant concentration ratio (R = 50) and lower temperatures and ferric ion concentrations, the 2,4-D conversion is lower than that obtained with R = 7. In this case, the hydrogen peroxide acts as a radical trapping agent, thus competing with the pollutant degradation path and rendering lower degradation rates[2] (Table 1, reaction step 3).

However, when T and $C_{Fe(III)}$ are increased for R = 50, the pollutant conversion is increased up to 100%.

4. PILOT-PLANT SOLAR REACTOR

4.1. Reactor Model. The solar experimental runs were performed in a pilot-plant solar reactor placed inside a batch recycling system that has a high-flow-rate centrifugal pump and a storage tank (Figure 3). Mass and thermal energy balances as well as its initial conditions are represented by the following expressions:[20]

$$\frac{\mathrm{d}}{\mathrm{d}t}\,\mathbf{C}(t) = \frac{V_{\mathrm{irr}}}{V}\langle \mathbf{R}(x,\,t)\rangle_{V_{\mathrm{irr}}} + \frac{V - V_{\mathrm{irr}}}{V}\mathbf{R}^{\mathrm{T}}(t) \tag{16}$$

$$\mathbf{C} = \mathbf{C}^0 \qquad t = 0 \tag{17}$$

$$\frac{\mathrm{d}}{\mathrm{d}t}\,T(t) = \Omega A_{\mathrm{c}} q_{\mathrm{T}}(t) - \Gamma[T - T_{\mathrm{a}}(t)] + \mathrm{K} \tag{18}$$

$$T = T^0 \qquad t = 0 \tag{19}$$

In eq 16, the first term on the right-hand side gives the degradation of the three reacting species (2,4-D, DCP, and P) produced by the irradiated (or photo-Fenton) reaction while the second one represents the decomposition of the same species generated by the nonirradiated (or Fenton) reaction. The required reaction rate expressions to be replaced in this equation are given by eqs 1−3 and 5.

The temperature evolution in the solar reactor is predicted by solving eqs 18 and 19, where T and T_{a} are the system and ambient air temperatures, A_{c} is the reactor window area, and q_{T} is the total broadband solar radiation flux incident on the reactor wall.[20] To take into account the variation of the solar zenith angle during the experimental runs, it should be noted that q_{T} is a function of time. In eq 18, the thermal energy parameters are defined by

Figure 3. View of the pilot-plant solar photoreactor.

$$\Omega = \frac{\eta_{\mathrm{o}}}{C_{\mathrm{T}}}, \qquad \Gamma = \frac{(\mathrm{UA})_{\mathrm{Tk}} + (\mathrm{UA})_{\mathrm{R}}}{C_{\mathrm{T}}}, \qquad \mathrm{K} = \frac{Q_{\mathrm{P}}}{C_{\mathrm{T}}} \tag{20}$$

Here η_{o} is the optical efficiency, $(\mathrm{UA})_{\mathrm{R}}$ and $(\mathrm{UA})_{\mathrm{Tk}}$ are the reactor and tank effective heat loss coefficients, Q_{P} is the constant heat input from the circulation pump, and C_{T} is the effective heat capacity of the reactor−tank system.

For the evaluation for the spectral LVRPA, it was assumed that the window of the reactor was irradiated with direct beam and diffuse solar radiation and that only radiation absorption in the reacting medium took place. Thus, the spectral LVRPA corresponding to the total solar radiation is given by

$$e^{\mathrm{a}}_{\lambda}(x,\,t) = e^{\mathrm{a}}_{\mathrm{B},\lambda}(x,\,t) + e^{\mathrm{a}}_{\mathrm{D},\lambda}(x,\,t) \tag{21}$$

where the direct beam (B) and diffuse (D) spectral LVRPA expressions are represented by

$$e^{\mathrm{a}}_{\mathrm{B},\lambda}(x,\,t) = \kappa_{\lambda}(t)\, q_{\mathrm{B},\lambda}(t)\, \Upsilon_{\mathrm{B},\lambda}(\mu_i)\, \exp[-\kappa_{\mathrm{T},\lambda}(t)x/\mu_{\mathrm{ref}}] \tag{22}$$

$$e^{\mathrm{a}}_{\mathrm{D},\lambda}(x,\,t) = 2\kappa_{\lambda}(t)\, q_{\mathrm{D},\lambda}(t)\, \Upsilon_{\mathrm{D},\lambda} E[x,\,\kappa_{\lambda}(t)] \tag{23}$$

dx.doi.org/10.1021/ie2023228 | Ind. Eng. Chem. Res. 2012, 51, 4181−4191

In eqs 22 and 23, $q_{B,\lambda}$ and $\Upsilon_{B,\lambda}$ are the direct beam radiation flux and transmittance for a given wavelength, $q_{D,\lambda}$ and $\Upsilon_{D,\lambda}$ are the diffuse radiation flux and transmittance for a given wavelength, κ_λ the spectral volumetric absorption coefficient of the absorbing species, $\kappa_{T,\lambda}$ the total absorption coefficient, and μ_{ref} and μ_i are the cosines of refraction and incident angles. In addition, in eq 23, $E(x,t)$ is the second-order exponential integral function.

The spectral direct beam transmittance is computed from:[32]

$$\Upsilon_{B,\lambda}(\mu_i) = \frac{\Upsilon_{1,\lambda}(\mu_i)\,\Upsilon_{2,\lambda}(\mu'_i)}{1 - \mathcal{R}_{1,\lambda}(\mu_i)\,\mathcal{R}_{2,\lambda}(\mu'_i)} \tag{24}$$

where $\Upsilon_{i,\lambda}$ and $\mathcal{R}_{i,\lambda}$ $(i = 1, 2)$ are the direct beam transmittance and reflectance for each plate:

$$\Upsilon_{i,\lambda} = \frac{\tau_\lambda(\mu_{ref})(1 - \rho_{nm})(1 - \rho_{uv})}{[1 - \tau_\lambda^2(\mu_{ref})\rho_{uv}\rho_{nm}]} \tag{25}$$

$$\mathcal{R}_{i,\lambda} = \rho_{nm} + \frac{\tau_\lambda^2(\mu_{ref})(1 - \rho_{nm})\rho_{uv}}{[1 - \tau_\lambda^2(\mu_{ref})\rho_{uv}\rho_{nm}]} \tag{26}$$

$$\tau_\lambda(\mu_{ref}) = \exp\left[-\kappa_\lambda(t)\frac{e}{\mu_{ref}}\right] \tag{27}$$

In eqs 25−27, ρ_{nm} and ρ_{uv} are the interface reflectivities and e is the plate thickness.

Finally, the spectral diffuse transmittance in eq 23 can be estimated as the spectral direct beam transmittance for a solar zenith angle equal to[33] 60°:

$$\Upsilon_D = \Upsilon_B[\mu_i = \cos(60°)] \tag{28}$$

4.2. Experiments. The nonconcentrating solar photoreactor is able to capture the UV/visible and near-infrared solar radiation[34] (Figure 3). The solution to be treated enters in a lower channel of the reactor, where it is preheated. Then the fluid circulates into an upper channel, where it is further heated, absorbs the UV/visible solar radiation, and makes use of this absorbed radiation for the pollutants degradation.

At the beginning of the experimental runs, the reactor window was covered with an opaque plate to avoid the entrance of solar radiation. Then ferric sulfate and 2,4-D aqueous solutions were added to the tank, and the pH was adjusted at 3.0. After that, the hydrogen peroxide solution was added to the tank and the first sample was withdrawn. Then, the reactor cover was removed to start the solar reaction.

During the experimental runs, the UV and total broadband solar radiation fluxes incident on the reactor window were measured by CUV3 and CM11 Kipp and Zonen radiometers. Reactor temperatures in different positions of the reactor were monitored with type J thermocouples. Besides, 2,4-D, DCP, TOC, hydrogen peroxide, and ferrous ions concentrations were analyzed with the procedure described in section 3.2.

Table 4 summarizes the operating conditions employed for irradiated and nonirradiated typical experimental runs to degrade 2,4-D in this photoreactor.

4.3. Predicted and Experimental Results. The model equations of the solar reactor were solved considering four computational steps for each value of the zenith angle: (i) computation of the spectral direct beam and diffuse solar radiation incident at the reactor window, (ii) evaluation of the spectral LVRPA (eqs 21−28), (iii) evaluation of the reaction rate for each of the reactant species (eqs 1 −3 and 5), and (iv) calculation of the 2,4-D, DCP, and H_2O_2 concentrations and reaction temperatures as a function of time (eqs 16−19). For the numerical solution, the Simple Model for the Atmospheric Radiative Transfer of Sunshine (SMARTS2) code[35] is called in every loop of the algorithm. In this way, the variations of the direct beam and diffuse solar radiation fluxes with the solar zenith angle are taken into account. More details on the numerical algorithm can be found in Farias et al.[20]

The SMARTS2 code predictions of the UV/visible and total solar radiation were obtained in Santa Fe, Argentina (31°39′ S, 60°43′ W, 8 m above sea level), on an inclined north-facing surface. The following input variables were considered to characterize the main atmospheric conditions: (i) the turbidity coefficients β of the Angstrom's turbidity formula were equal to 0.055 and 0.085; (ii) the wavelength exponents α_1 and α_2 for the Angstrom approach were adopted from a reference rural-aerosol model tabulated for different relative humidities;[35] (iii) a value of 0.815 was adopted for the aerosol single scattering albedo for the UV/visible wavelength range (280−450 nm), and a value of 0.95 was adopted for the total wavelength range;[36] and (iv) an aerosol asymmetry factor equal to 0.65 was assumed for any wavelength.[37]

Table 5 summarizes the pilot-plant reactor, solar radiation, optical, and thermal energy parameters used to solve the reactor model.

Figure 4 depicts a 3-D representation of typical computed results of LVRPA for a zenith angle equal to 28°, as a function of the ferric ion concentrations and the position x inside the solar reactor. As is shown in the figure, the photon absorption rate presents a marked variation along the x-coordinate for higher Fe(III) concentrations. For example, for an initial ferric ion concentration $C^0_{Fe^{3+}}$ = 5.0 ppm, approximately 53% of the solar radiation is absorbed for a reactor thickness equal to 30 mm.

Experimental results for irradiated (runs 1−3) and nonirradiated (run 4) experiments are presented in Table 4. Conversions of 2,4-D after a reaction time of 30 min and of TOC after 30 and 210 min are reported. TOC experimental conversions after 210 min of operation were performed to ensure not only the degradation of the 2,4-D and DCP but also the aliphatic intermediates that are not detected by HPLC (see, for example, the high TOC conversions achieved for runs 2 and 3). Concerning the ability of the reactor to capture the near-infrared solar radiation, it can be noted that a temperature increase of 21 °C was observed for an irradiated experiment after 210 min (run 3), while it was only 7.9 °C under a nonirradiated condition and the same reaction time (run 4).

Figure 5 shows model predictions and experimental data as a function of time for the temperature in the storage tank (Figure 5a), the UV broadband solar radiation (Figure 5b), and the total broadband solar radiation (Figure 5c). Considering the irradiated and nonirradiated runs, it is noted that a good representation of the experimental results was achieved with the solar reactor model; the root-mean-square error (RMSE) of the temperature and UV and total radiation predictions were 1.4 °C, 3.4 W m^{-2}, and 9.3 W m^{-2}, respectively.

Predicted and experimental 2,4-D, DCP, and H_2O_2 concentrations are shown in Figure 6. The effect of UV solar radiation and high temperatures on herbicide degradation can be observed by comparison of parts a and b of Figure 6 (runs 4 and 1). These experiments were performed by a constant initial pollutant concentration ($C^0_{2,4\text{-}D}$ = 0.13 mM) and similar values

dx.doi.org/10.1021/ie2023228 | Ind. Eng. Chem. Res. 2012, 51, 4181−4191

Table 4. Typical Experimental Runs for $C^0_{2,4\text{-D}}$ = 0.13 mM and experimental conversions of 2,4-D and TOC

no.	reaction	$C^0_{Fe^{3+}}$(ppm)	$C^0_P/C^0_{2,4\text{-D}}$	initial LST[a]	T^0 (°C)	ΔT^{210} (°C)	$X^{30}_{2,4\text{-D}}$(%)	X^{30}_{TOC}(%)	X^{210}_{TOC}(%)
1	irradiated	2.8	31.5	12:40	28	15.3	95.1	22.7	91.6
2	irradiated	1.0	30.5	12:50	31	17.9	61.7	10.6	98.9
3	irradiated	1.0	24.6	10:50	33	21.0	59.7	4.6	98.6
4	nonirradiated	3.0	31.6	12:50	30	7.9	39.1	7.6	44.6

[a]LST, local standard time.

Table 5. Pilot-Plant Solar Reactor and Model Parameters

parameter	value	unit
Solar Reactor		
window area (A_c)	0.24	m^2
reactor depth (L)	30.00	mm
plate thickness (e)	3.20	mm
irradiated volume (V_{irr})	6.10	dm^3
total liquid volume (V)	35.00	dm^3
Solar Radiation		
UV/visible spectral range	280−450	nm
total radiation spectral range	305−2800	nm
tilt angle	30	deg
azimuth angle counted clockwise from north	0	deg
Optical		
transmittance of acrylic windows	0.60−0.90[a]	
polycarbonate plate refractive index	1.49	
water refractive index	1.33	
air refractive index	1.00	
Thermal		
optical efficiency/effective heat capacity (Ω)	$(9.10 \pm 0.51) \times 10^{-5}$	$°C J^{-1}$
heat loss/effective heat capacity (Γ)	$(5.39 \pm 0.21) \times 10^{-6}$	s^{-1}
heat input from the pump/effective heat capacity (K)	$(8.28 \pm 0.40) \times 10^{-4}$	$°C s^{-1}$

[a]It is a function of wavelength.[16]

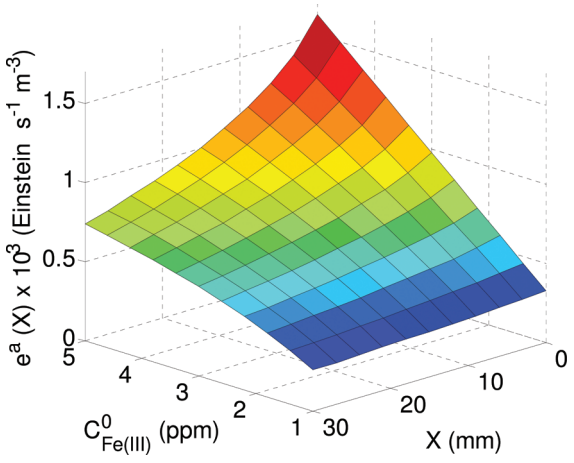

Figure 4. Typical simulated results of LVRPA for θ_z = 28°, as a function of the ferric ion concentrations and the position x inside the solar reactor.

of ferric ion concentrations ($C^0_{Fe^{3+}}$ = 3.0 and 2.8 ppm), hydrogen peroxide to pollutant initial molar ratios (R = 31.6 and 31.5), and initial reaction temperatures (T^0 = 30 and 28 °C). After 30 min of reaction time, the following pollutant conversions are observed: $X^{30}_{2,4\text{-D}}$ = 39.1% for run 4 and $X^{30}_{2,4\text{-D}}$ = 95.1% for run 1. Thus, an enhancement of 143% in the 2,4-D conversion has been achieved under irradiated conditions.

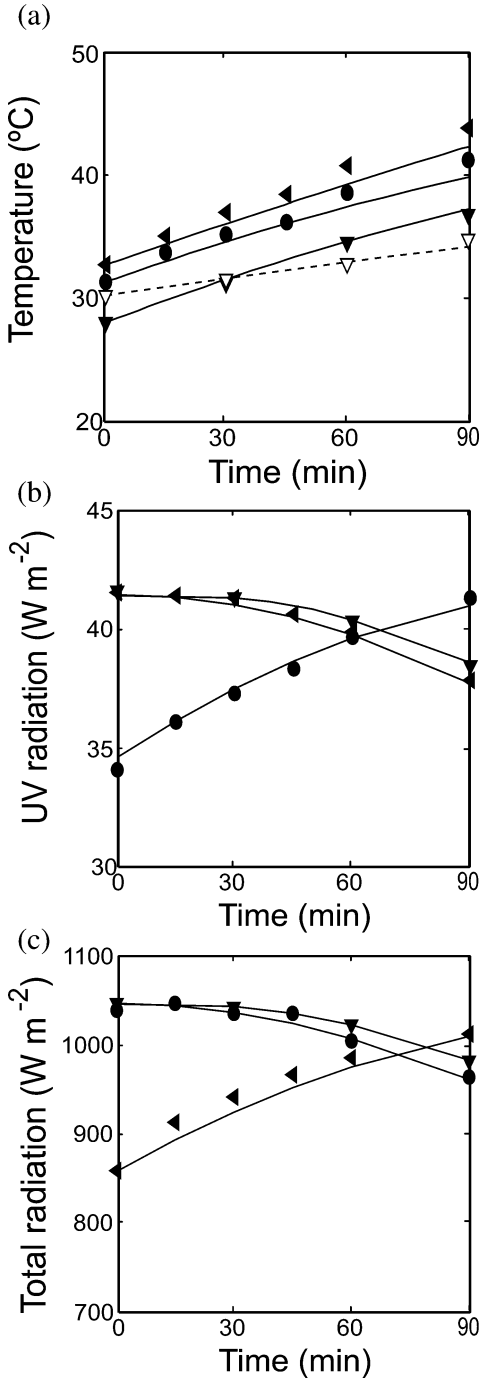

Figure 5. Model predictions (lines) and experimental data (symbols) vs time: (a) temperatures in the storage tank, (b) UV broadband solar radiation, and (c) total broadband solar radiation. Keys for irradiated experiments: run 1 (—,▼), run 2 (—,●), and run 3 (—, ◀). Key for the nonirradiated experiment (---,▽).

The effect of the ferric ion concentration on photo-Fenton treatment is shown in Figure 6b,c (runs 1 and 2). These

dx.doi.org/10.1021/ie2023228 | Ind. Eng. Chem. Res. 2012, 51, 4181−4191

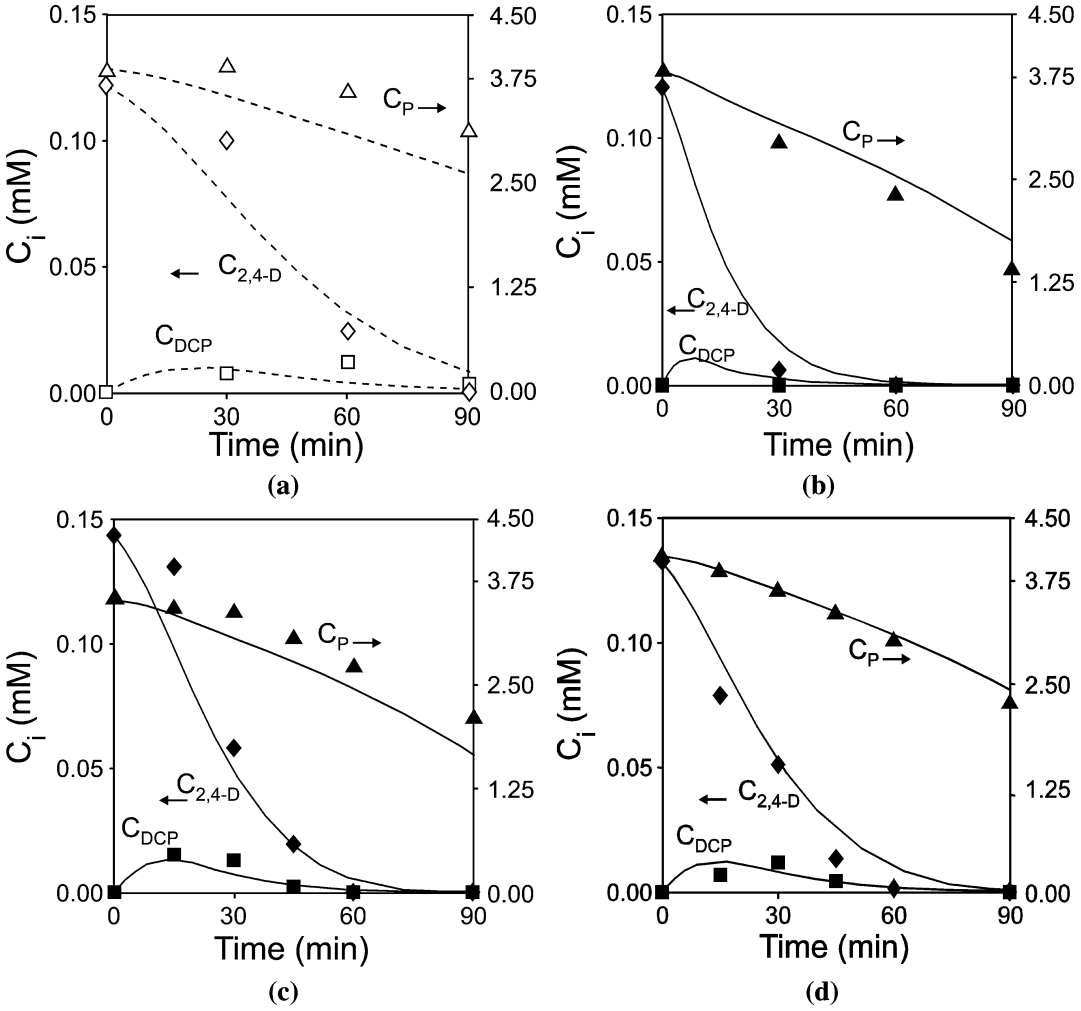

Figure 6. Model predictions (lines) and experimental (symbols) concentrations vs time for $C^0_{2,4\text{-D}}$ = 0.13 mM. (a) Nonirradiated experiment: $C^0_{Fe^{3+}}$ = 3.0 ppm, R = 31.6, T^0 = 30 °C. (b) Irradiated experiment: $C^0_{Fe^{3+}}$ = 2.8 ppm, R = 31.5, T^0 = 28 °C. (c) Irradiated experiment: $C^0_{Fe^{3+}}$ = 1.0 ppm, R = 30.5, T^0 = 31. (d) Irradiated experiment: $C^0_{Fe^{3+}}$ = 1.0 ppm, R = 24.6, T^0 = 33 °C. Keys for photo-Fenton: 2,4-D (◆), DCP (■), hydrogen peroxide (▲). Keys for Fenton: 2,4-D (◇), DCP (□), hydrogen peroxide (Δ).

experiments were carried out by similar initial temperatures (T^0 = 28 and 31 °C) and hydrogen peroxide to pollutant initial molar ratios (R = 31.5 and 30.5) and two different ferric ion concentrations ($C^0_{Fe^{3+}}$ = 2.8 and 1.0 ppm). A more efficient pollutant degradation at the highest ferric iron concentration was observed. The 2,4-D conversion after 30 min and at $C^0_{Fe^{3+}}$ = 2.8 ppm was 95.1%, while it was only 61.7% when the lowest ferric ion concentration was used. A similar effect of the ferric ion concentration was observed for the TOC conversion for a reaction time of 30 min. However, for a reaction time equal to 210 min, the TOC conversion is slightly higher for a ferric ion concentration equal to 1.0 ppm; these results can be explained by a total depletion of the hydrogen peroxide for run 1 after a reaction time of 210 min.

Finally, two runs for an equal ferric ion concentration ($C^0_{Fe^{3+}}$ = 1.0 ppm) and rather similar initial local standard times (LST = 12:50 and 10:50) and hydrogen peroxide to pollutant initial molar ratios (R = 30.5 and 24.6) are compared in parts c and d of Figure 6 (runs 2 and 3). For these experiments, it should be noted that a comparable degradation rate was achieved and that hydrogen peroxide is not completely consumed. Besides, the largest mineralization (X^{210}_{TOC} = 98.9 and 98.6%) was reached after 210 min (Table 4).

As shown from the irradiated experimental runs, this solar pilot-plant photoreactor was able to reach a complete degradation of the 2,4-D and DCP after 60 min of treatment, as well as a very high mineralization of the herbicide after 210 min.

5. CONCLUSIONS

A pilot-plant solar reactor model was presented and experimentally validated to study the photo-Fenton degradation of the herbicide 2,4-dichlorophenoxyacetic acid (2,4-D) in aqueous solution. First, the results of a proposed kinetic model and the experimental data obtained in a well-stirred tank laboratory reactor were employed to estimate the main kinetic parameters. In order to compute the concentrations of the herbicide 2,4-D, the intermediate compound 2,4-dichlorophenol (DCP), and hydrogen peroxide, as well as the reaction temperature as a function of time, the mass and thermal energy balances were solved.

Afterward, the kinetic model was used to study the photo-Fenton process in a pilot-plant solar reactor, specially

dx.doi.org/10.1021/ie2023228 | Ind. Eng. Chem. Res. 2012, 51, 4181–4191

constructed to capture the UV/visible and IR solar radiation. Predictions of the temperature in the storage tank and of the UV and total broadband solar radiation fluxes incident on the reactor window were compared with experimental data, and a satisfactory agreement was found. The root-mean-square error of the temperature and UV and total radiation predictions were 1.4 °C, 3.4 W m^{-2}, and 9.3 W m^{-2}, respectively. Besides, due to the ability of the reactor to capture the infrared solar radiation, a temperature increase up to 21 °C was reached for irradiated experiments.

The effect of different operating parameters of the solar photo-Fenton process, such as solar radiation fluxes, ferric ion concentrations, and initial local standard times, on the herbicide degradation was also studied. Comparing the experimental results after 30 min under dark and irradiated conditions, an enhancement of 143% in the 2,4-D conversion was achieved. For experiments with solar radiation and a reaction time of 60 min, the pilot-plant reactor was able to reach an almost complete degradation of the herbicide 2,4-D and 2,4-dichlorophenol. In addition, after 210 min of treatment and similar operating conditions, the total organic carbon (TOC) conversion was of 98.9%.

APPENDIX A

Considering the assumptions i−v proposed in section 2 for the kinetic model, the reaction rates for the n reacting species ($n = 8$) may be written by the following matrix representation:

$$\mathbf{R}(x,t) = \mathbf{S}\cdot\mathbf{K}'(x,t) \tag{A.1}$$

Here $\mathbf{R}(x,t)$ is the array of reaction rates for the n reacting species, $\mathbf{S}$ the stoichiometry matrix, and $\mathbf{K}'(x,t)$ the array of the reaction rates of each elementary step determined by the law of mass action. Equation A.1 may be also represented by

$$\mathbf{R}(x,t) = \begin{bmatrix} R_{2,4\text{-D}}(x,t) \\ R_{\text{DCP}}(x,t) \\ R_{\text{QH}_2}(x,t) \\ R_{\text{Fe}^{2+}}(x,t) \\ R_{\text{Fe}^{3+}}(x,t) \\ R_{\text{P}}(x,t) \\ R_{\text{OH}^\bullet}(x,t) \\ R_{\text{QH}^\bullet}(x,t) \end{bmatrix} = \begin{bmatrix} 0 & 0 & 0 & -1 & 0 & 0 & 0 & 0 \\ 0 & 0 & 0 & 1 & -1 & 0 & 0 & 0 \\ 0 & 0 & 0 & 0 & 1 & -1 & 0 & 0 \\ 1 & -1 & 0 & 0 & 0 & 1 & 1 & 1 \\ -1 & 1 & 0 & 0 & 0 & -1 & -1 & -1 \\ -1 & -1 & -1 & 0 & 0 & 0 & 0 & 0 \\ 0 & 1 & -1 & -1 & -1 & 0 & 0 & 1 \\ 0 & 0 & 0 & 0 & 0 & 1 & -1 & 0 \end{bmatrix} \times \begin{bmatrix} k_1 C_{\text{Fe}^{3+}} C_{\text{P}} \\ k_2 C_{\text{Fe}^{2+}} C_{\text{P}} \\ k_3 C_{\text{OH}^\bullet} C_{\text{P}} \\ k_{11} C_{\text{OH}^\bullet} C_{2,4\text{-D}} \\ k_{12} C_{\text{OH}^\bullet} C_{\text{DCP}} \\ k_{14} C_{\text{QH}_2} C_{\text{Fe}^{3+}} \\ k_{15} C_{\text{QH}^\bullet} C_{\text{Fe}^{3+}} \\ \bar{\Phi}_{\text{Fe(II)}} \sum_\lambda e^{\text{a}}_\lambda(x) \end{bmatrix} \tag{A.2}$$

where

$$R_{\text{Fe}^{2+}}(x,t) = -R_{\text{Fe}^{3+}}(x,t) \tag{A.3}$$

Here $R_i(x,t)$ are the reaction rates and C_i the molar concentrations for i species (i = 2,4-D, DCP, QH_2, Fe^{2+}, Fe^{3+}, P, $OH^\bullet$, $QH^\bullet$), $\bar{\Phi}_{\text{Fe(II)}}$ is the wavelength averaged primary quantum yield, and $e^{\text{a}}_\lambda(x)$ is the spectral local volumetric rate of photon absorption (LVRPA).

Equation A.2 is solved to obtain the mathematical expressions of $R_i(x,t)$. To do this, the steady state approximation (SSA) may be applied for highly reactive radicals and species with very low concentrations,

$$R_{\text{QH}^\bullet}(x,t) = k_{14} C_{\text{QH}_2} C_{\text{Fe}^{3+}} - k_{15} C_{\text{QH}^\bullet} C_{\text{Fe}^{3+}} = 0 \tag{A.4}$$

$$R_{\text{OH}^\bullet}(x,t) = \bar{\Phi}_{\text{Fe(II)}} \sum_\lambda e^{\text{a}}_\lambda(x) + k_2 C_{\text{Fe}^{2+}} C_{\text{P}} - k_3 C_{\text{OH}^\bullet} C_{\text{P}} - k_{11} C_{\text{OH}^\bullet} C_{2,4\text{-D}} - k_{12} C_{\text{OH}^\bullet} C_{\text{DCP}} = 0 \tag{A.5}$$

$$R_{\text{QH}_2}(x,t) = k_{12} C_{\text{OH}^\bullet} C_{\text{DCP}} - k_{14} C_{\text{QH}_2} C_{\text{Fe}^{3+}} = 0 \tag{A.6}$$

$$R_{\text{Fe}^{2+}}(x,t) = \bar{\Phi}_{\text{Fe(II)}} \sum_\lambda e^{\text{a}}_\lambda(x) + k_1 C_{\text{Fe}^{3+}} C_{\text{P}} - k_2 C_{\text{Fe}^{2+}} C_{\text{P}} + k_{14} C_{\text{QH}_2} C_{\text{Fe}^{3+}} + k_{15} C_{\text{QH}^\bullet} C_{\text{Fe}^{3+}} = 0 \tag{A.7}$$

From eqs A.4 and A.6, it can be shown that

$$k_{12} C_{\text{DCP}} C_{\text{OH}^\bullet} = k_{14} C_{\text{QH}_2} C_{\text{Fe}^{3+}} = k_{15} C_{\text{QH}^\bullet} C_{\text{Fe}^{3+}} \tag{A.8}$$

Then, by replacing eq A.8 into eq A.7 and solving the equation system obtained from eqs A.5 and A.7, the following expression can be derived

$$C_{\text{Fe}^{2+}} = \left(\frac{\bar{\Phi}_{\text{Fe(II)}} \sum_\lambda e^{\text{a}}_\lambda(x) \left(1 + 2\frac{k_{12} C_{\text{DCP}}}{\alpha_1}\right) + k_1 C_{\text{Fe}^{3+}} C_{\text{P}}}{k_2 C_{\text{P}} \left(1 - 2\frac{k_{12} C_{\text{DCP}}}{\alpha_1}\right)} \right) \tag{A.9}$$

where

$$\alpha_1 = k_3 C_{\text{P}} + k_{11} C_{2,4\text{-D}} + k_{12} C_{\text{DCP}} \tag{A.10}$$

From eqs A.5, A.9, and A.10,

$$C_{\text{OH}^\bullet} = \left(\frac{2\bar{\Phi}_{\text{Fe(II)}} \sum_\lambda e^{\text{a}}_\lambda(x) + k_1 C_{\text{Fe}^{3+}} C_{\text{P}}}{\alpha_1 - 2k_{12} C_{\text{DCP}}} \right) \tag{A.11}$$

Then, from eqs A.2 and A.11 and recalling that $K_1 = k_1$, the final expression for the 2,4-D reaction rate is

$$R_{2,4\text{-D}}(x,t) = -k_1 C_{\text{OH}^\bullet} C_{2,4\text{-D}}$$

$$R_{2,4\text{-D}}(x,t) = R^{\text{T}}_{2,4\text{-D}}(t) + \bar{\Phi}_{\text{Fe(II)}} \sum_\lambda e^{\text{a}}_\lambda(x) \left(-\frac{2}{\delta}\right)$$

$$R^{\text{T}}_{2,4\text{-D}}(t) = K_1 C_{\text{Fe}^{3+}} C_{\text{P}} \left(-\frac{1}{\delta}\right)$$

The same procedure may be used to derive the reaction rates for DCP and P (eq 1 of the main body of the paper).

dx.doi.org/10.1021/ie2023228 | Ind. Eng. Chem. Res. 2012, 51, 4181−4191

AUTHOR INFORMATION

Corresponding Author

*Fax: +54 342 4511087. E-mail: alfano@intec.unl.edu.ar.

Notes

The authors declare no competing financial interest.

ACKNOWLEDGMENTS

The authors are grateful to Universidad Nacional del Litoral (UNL), Consejo Nacional de Investigaciones Científicas y Técnicas (CONICET), and Agencia Nacional de Promoción Científica y Tecnológica (ANPCyT). They also thank Tec. Antonio C. Negro and Eng. Alejandra Barlatey for valuable help during the experimental work.

NOMENCLATURE

A_1	reparameterized parameter
A_c	window area, m^2
B_1	reparameterized parameter
C	molar concentration, M
C_T	effective heat capacity of the reactor−tank system, J $°C^{-1}$
e	plate thickness, m
e^a	local volumetric rate of photon absorption (LVRPA), einstein cm^{-3} s^{-1}
E	activation energy, kJ mol^{-1}
f	normalized spectral distribution of the lamp output power
k_i	kinetic constant, M^{-1} s^{-1}
K_i	kinetic parameter, dimensional or dimensionless
L	reactor depth, m
n	refractive index, dimensionless
q	net radiative flux, einstein cm^{-2} s^{-1}
Q_P	heat input from the pump, J s^{-1}
R	hydrogen peroxide to 2,4-D initial concentration ratio, dimensionless
$R_{subscript}$	reaction rate, M s^{-1}
R'	ideal gas constant, kJ mol^{-1} K^{-1}
$\mathcal{R}$	reflectance, dimensionless
T	absolute temperature,K
t	time, s
UA	effective heat loss coefficient, J $°C^{-1}$ s^{-1}
V	volume, m^3
x	spatial coordinate, m
X	conversion, dimensionless
X_i	coded variable

Greek Letters

α	molar absorptivity, m^2 mol^{-1}
δ	dimensionless function defined in eq 2
η_o	optical efficiency, dimensionless
θ_z	solar zenith angle, deg
κ	volumetric absorption coefficient, m^{-1}
K	ratio of heat input from the pump to effective heat capacity, °C s^{-1}
λ	wavelength, nm
μ	the quantity cos θ, dimensionless
ρ	reflectivity, dimensionless
Υ	transmittance, dimensionless
Γ	ratio of heat loss to effective heat capacity, s^{-1}
$\mathbf{\Gamma}(t)$	function defined in eq 4
Φ	primary quantum yield, mol $einstein^{-1}$
Ω	ratio of optical efficiency to effective heat capacity, °C J^{-1}

Subscripts

a	air property
B	relative to direct beam radiation
D	relative to diffuse radiation
2,4-D	relative to 2,4-dichlorofenoxiacetic acid
DCP	relative to 2,4-dichlorophenol
Fe^{2+}	relative to ferrous ion
Fe^{3+}	relative to ferric ion
i	incident radiation
irr	relative to an irradiated property
P	relative to hydrogen peroxide
ref	refracted radiation
R	relative to the reactor
T	total
Tk	tank property
w	wall property
λ	indicates a dependence on wavelength
∞	relative to pre-exponential factor

Superscripts

0	initial condition
T	thermal rate

Special Symbols

$\langle\rangle$	average value

REFERENCES

(1) Bedoui, A.; Elalaoui, L.; Abdel-Wahab, A.; Bensalah, N. Photo-Fenton treatment of actual agro-industrial wastewaters. *Ind. Eng. Chem. Res.* **2011**, *50*, 6673.

(2) Pignatello, J. J.; Oliveros, E.; MacKay, A. Advanced oxidation processes for organic contaminant destruction based on the Fenton reaction and related chemistry. *Crit. Rev. Environ. Sci. Technol.* **2006**, *36*, 1.

(3) Sagawe, G.; Lehnard, A.; Lübber, M.; Bahnemann, D. The insulated solar Fenton hybrid process: Fundamental investigations. *Helv. Chim. Acta* **2001**, *84*, 3742−3759.

(4) Gernjak, W.; Fuerhacker, M.; Fernández-Ibáñez, P.; Blanco, J.; Malato, S. Solar photo-Fenton treatment-process parameters and process control. *Appl. Catal. B Environ.* **2006**, *64* (1−2), 121−130.

(5) Farias, J.; Albizzati, E. D.; Alfano, O. M. Kinetic study of the photo-Fenton degradation of formic acid. Effects of temperature and iron concentration. *Catal. Today.* **2009**, *144*, 117.

(6) Chen, R.; Pignatello, J. J. Role of quinone intermediates as electron shuttles in Fenton and photoassisted Fenton oxidations of aromatic compounds. *Environ. Sci. Technol.* **1997**, *31*, 2399.

(7) Chen, F.; Ma, W.; He, J.; Zhao, J. Fenton degradation of malachite green catalyzed by aromatic additives. *J. Phys. Chem. A* **2002**, *106*, 9485.

(8) Nichela, D.; Carlos, L.; García Einschlag, F. Autocatalytic oxidation of nitrobenzene using hydrogen peroxide and Fe(III). *Appl. Catal. B Environ.* **2008**, *82*, 11.

(9) Nichela, D.; Haddou, M.; Benoit-Marquié, F.; Maurette, M.; Oliveros, E.; García Einschlag, F. S. Degradation kinetics of hydroxy and hydroxynitro derivatives of benzoic acid by Fenton-like and photo-Fenton techniques: A comparative study. *Appl. Catal. B: Environ.* **2010**, *98*, 171.

(10) Malato, S.; Fernández-Ibáñez, P.; Maldonado, M. I.; Blanco, J.; Gernjak, W. Decontamination and disinfection of water by solar photocatalysis: Recent overview and trends. *Catal. Today.* **2009**, *147*, 1.

(11) Rodriguez, M.; Malato, S.; Pulgarin, C.; Contreras, S.; Curco, D.; Gimenez, J.; Esplugas, S. Optimizing the solar photo-Fenton process in the treatment of contaminated water. Determination of intrinsic kinetic constants for scale-up. *Sol. Energy* **2005**, *79*, 360.

(12) Shawaqfeh, A. T.; Al Momani, F. A. Photocatalytic treatment of water soluble pesticide by advanced oxidation technologies using UV light and solar energy. *Sol. Energy* **2010**, *84*, 1157.

(13) Pérez-Estrada, L.; Malato, S.; Gernjak, W.; Agüera, A.; Thurman, E. M.; Ferrer, I.; Fernández-Alba, A. R. Photo-Fenton degradation of diclofenac: Identification of main intermediates and degradation pathway. *Environ. Sci. Technol.* **2005**, *39*, 8300.
(14) Radjenovic, J.; Sirtori, C.; Petrovic, M.; Barcelo, D.; Malato, S. Solar photocatalytic degradation of persistent pharmaceuticals at pilot-scale: Kinetics and characterization of major intermediate products. *Appl. Catal. B: Environ.* **2009**, *89*, 255.
(15) Zapata, A.; Oller, I.; Bizani, E.; Sánchez-Pérez, J. A.; Maldonado, M. I.; Malato, S. Evaluation of operational parameters involved in solar photo-Fenton degradation of a commercial pesticide mixture. *Catal. Today.* **2009**, *144*, 94.
(16) Mendoza-Marín, C.; Osorio, P.; Benítez, N. Decontamination of industrial wastewater from sugarcane crops by combining solar photo-Fenton and biological treatments. *J. Hazard. Mater.* **2010**, *177*, 851.
(17) Jiménez, M.; Oller, I.; Maldonado, M. I.; Malato, S.; Hernández-Ramírez, A.; Zapata, A.; Peralta-Hernández, J. M. Solar photo-Fenton degradation of herbicides partially dissolved in water. *Catal. Today.* **2011**, *161*, 214.
(18) Monteagudo, J. M.; Durán, M.; San Martín, I.; Aguirre, M. Effect of continuous addition of H_2O_2 and air injection on ferrioxalate-assisted solar photo-Fenton degradation of Orange II. *Appl. Catal. B: Environ.* **2009**, *89*, 510.
(19) Klamerth, N.; Malato, S.; Maldonado, M. I.; Agüera, A.; Fernández-Alba, A. R. Application of photo-Fenton as a tertiary treatment of emerging contaminants in municipal wastewater. *Environ. Sci. Technol.* **2010**, *44*, 1792.
(20) Farias, J.; Albizzati, E. D.; Alfano, O. M. New pilot-plant photo-Fenton solar reactor for water decontamination. *Ind. Eng. Chem. Res.* **2010**, *49*, 1265.
(21) Sun, Y.; Pignatello, J. J. Photochemical reactions in the total mineralization of 2,4-D by $Fe^{3+}/H_2O_2/UV$. *Environ. Sci. Technol.* **1993**, *27*, 304.
(22) Sun, Y.; Pignatello, J. J. Organic intermediates in the degradation of 2,4-dichlorophenoxyacetic acid by Fe^{3+}/H_2O_2 and $Fe^{3+}/H_2O_2/UV$. *J. Agric. Chem.* **1993**, *41*, 1139.
(23) Brillas, E.; Calpe, J. C.; Casado, J. Mineralization of 2,4-D by advanced electrochemical oxidation processes. *Water Res.* **2000**, *34*, 2253.
(24) Alfano, O. M.; Romero, R. L.; Cassano, A. E. A cylindrical photoreactor irradiated from the bottom. I. Radiation flux density generated by a tubular source and a parabolic reflector. *Chem. Eng. Sci.* **1985**, *40*, 2119.
(25) Faust, B. C.; Hoigné, J. Photolysis of Fe(III)−hydroxy complexes as sources of OH radicals in clouds, fog and rain. *Atmos. Environ.* **1990**, *24A*, 79.
(26) Farias, J.; Rossetti, G. H.; Albizzati, E. D.; Alfano, O. M. Solar degradation of formic acid: Temperature effects on the photo-Fenton reaction. *Ind. Eng. Chem. Res.* **2007**, *46*, 7580.
(27) Sapieszko, R. S.; Patel, R. C.; Matijevic, E. J. Ferric hydrous oxide sols. 2. Thermodynamics of aqueous hydroxo and sulfato ferric complexes. *Phys. Chem.* **1977**, *81*, 1061.
(28) Esterkin, C. R.; Negro, A. C.; Alfano, O. M.; Cassano, A. E. Air pollution remediation in a fixed bed photocatalytic reactor coated with TiO_2. *AIChE J.* **2005**, *51*, 2298−2310.
(29) Coonick, W. J.; Simoneaux, J. M. Determination of (2,4-dichlorophenoxy)acetic acid and 2,6-dichlorobenzonitrile in water by high-performance liquid chromatography. *J. Agric. Food. Chem.* **1982**, *30*, 258.
(30) Murov, S. L.; Carmichael, I.; Hug, G. L. *Handbook of Photochemistry*, 2nd ed., Marcel Dekker: New York, 1993; pp 299−305.
(31) Schwaab, M.; Pinto, J. C. Optimum reference temperature for reparameterization of the Arrhenius equation. Part 1: Problems involving one kinetic constant. *Chem. Eng. Sci.* **2007**, *62*, 2750.
(32) Siegel, R.; Howell, J. R. *Thermal Radiation Heat Transfer*, 4th ed.; Taylor & Francis: Washington, DC, 2002.
(33) Duffie, J. A.; Beckman, W. *Solar Engineering of Thermal Processes*, 2nd ed.; John Wiley & Sons: New York, 1991.
(34) Farias, J.; Rossetti, G. H.; Albizzati, E. D.; Alfano, O. M. Reactor solar para descontaminación de aguas. Argentine Patent Office P-080103697. *Argentine Patent Office Bulletin* **2009**, *559*.
(35) Gueymard, C. *SMARTS2, a Simple Model of the Atmospheric Transfer of Sunshine: Algorithms and Performance Assessment*; Report FSEC-PF-270-95; Florida Solar Energy Center: Cocoa, FL, 1995.
(36) Piacentini, R.; Alfano, O. M.; Albizzati, E. D.; Luccini, E.; Herman, J. Solar ultraviolet irradiance for clear sky days incident at Rosario, Argentina: Measurements and model calculations. *J. Geophys. Res.* **2002**, *107*, 6.
(37) Bird, R. E.; Riordan, C. Simple spectral model for direct and diffuse irradiance on horizontal and tilted planes at the Earth's surface for cloudless atmospheres. *J. Clim. Appl. Meteorol.* **1986**, *25*, 87.